Inversion of seismic data with different time axis, 4D and PP/PS example

Olivier Colnard, Santan Kumar, Benjamin Roure CGG

Introduction

Seismic inversion is now a standard tool to extract quantitative information from the amplitude. This technique initially used to derive acoustic impedance from a single stack seismic data has evolved to be able to handle simultaneously several seismic volumes that can be pre stack, azimuthal, PP/PS or time lapse for example. Classically only one time axis was considered and preconditioning of the seismic data in the case of PP/PS or time lapse was required to align the different seismic volumes to a same reference prior to inversion.

This paper describes an innovative inversion scheme that is able to handle several seismic data with different time axis. The benefit of this technique is illustrated with two examples, one on time lapse seismic and one on PP/PS.

Method

Coulon et al. (2006) described a non-linear inversion where PP angle stacks are inverted using a simulated annealing optimization technique. This model-based inversion is defined in a stratigraphic grid which consists of layers defined in time and consistent with the geology and seismic dips. The thickness of the layers is controlled by the wavelet bandwidth. Each cell of the grid contains values describing the P-velocity, V_P, S-velocity, V_S, density, ρ, and time position of the layers, T. These properties are iteratively perturbed in order to minimize a three term cost function where the first term measures the misfit between the real seismic amplitudes and the synthetic amplitudes calculated by 1D convolution of the reflectivities using angle-dependent wavelets. The second term of the objective function imposes lateral and vertical continuity constraints which control the smoothness of the inverted elastic properties in the presence of noise. The last term in the cost function controls how far the solution is allowed to move away from a user-specified, low-frequency initial model.

In the case where a 4D inversion is performed the stratigraphic grid provides a natural framework to handle time shifts (Lafet et al., 2009; Michou et al., 2013). We have the possibility to link between consecutive vintages Vp variations, ΔVp, and time shifts, Δt, of each cell and thus to derive monitor time from the ΔVp Base/Monitor ratio. Each vintage has a specific time axis (layer position) whose consistency with other vintages is ensured by the inversion process and its cost function

The stratigraphic inversion method can also easily be extended to a joint inversion (Roure et al., 2015) by adding PS angle stacks in PS times and their associated angle-dependent wavelets (with lower frequency than the PP wavelets). The travel time difference between PP and PS data is handled by defining two time axis in the stratigraphic grid, T_{PP} and T_{PS}, linked by the V_P/V_S ratio through the relation (Anderson and Lines, 2008):

$$\frac{V_P}{V_S} = 2\frac{\Delta T_{PS}}{\Delta T_{PP}} - 1 \qquad (1)$$

where ΔT represents the thickness of the layers in PP or PS times.
The amplitudes misfit term of the cost function is modified to account simultaneously for the PP and PS data misfit in their respective time domain. The PP and PS reflectivities are computed using the Zoeppritz equations (1919) or Aki and Richards approximations (1980) whose simplified expression at an interface between two isotropic elastic media for a given angle of incidence is:

$$R_{PP} = a\frac{\Delta V_P}{\overline{V_P}} + b\frac{\Delta V_S}{\overline{V_S}} + c\frac{\Delta \rho}{\overline{\rho}} \qquad (2)$$

$$R_{PS} = d\frac{\Delta V_S}{\bar{V}_S} + e\frac{\Delta^\circ}{\bar{\sigma}} \quad (3)$$

where Δ and $\bar{}$ are respectively the difference and the average of the properties above and below the interface, and the parameters *a*, *b*, *c*, *d* and *e* are combinations of elastic properties and angles of incidence and reflection. The benefits of including the PS reflectivity for AVO inversion are discussed in Gray (2003).

We now have a set of three equations (1-3) to invert simultaneously amplitudes and travel times. Including the travel times as part of the inversion brings extra constraints on the inverted V_P/V_S ratio. During inversion, a V_P/V_S perturbation will introduce a vertical shift in layer position in PS time. The iterative perturbation process will automatically optimize the alignment between synthetic and real data in PS time as well as the amplitudes match.

4D example

The 4D methodology was applied on a synthetic and real dataset. First an exercise on synthetic data was performed to assess the impact of stretching the monitor on the AVO response illustrated in Figures 1 and 2.

A simple blocky model composed of a reservoir layer of 15 ms was built with a constant velocity of 2500 m/s for the Base case in black. For the monitor scenario in blue the velocity has been decreased by 15% creating a time shift of 2.64 ms. The curve in red corresponds to the monitor scenario stretched to the time of the base. A synthetic gather was calculated for each case.

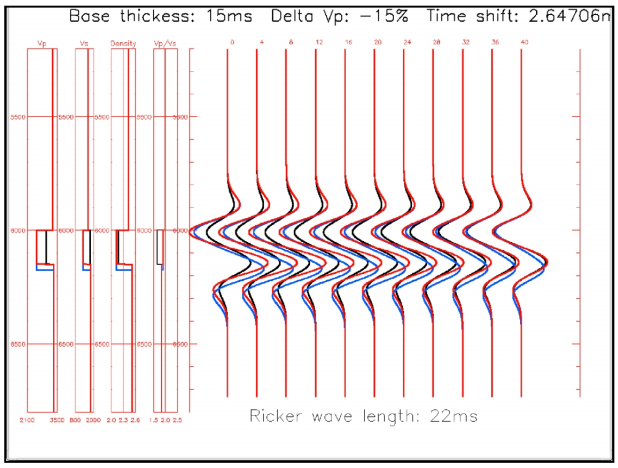

Figure 1: AVO modelling for a base and monitor case

The impact of the stretching AVO effect is analysed by computing the ratio between the peak and trough amplitude. We can observe in Figure 2 that the AVO response is different for the monitor before and after stretch (blue and red curves). Therefore because of interferences between top and base, inversion will not recover the correct elastic contrasts from stretched monitor.

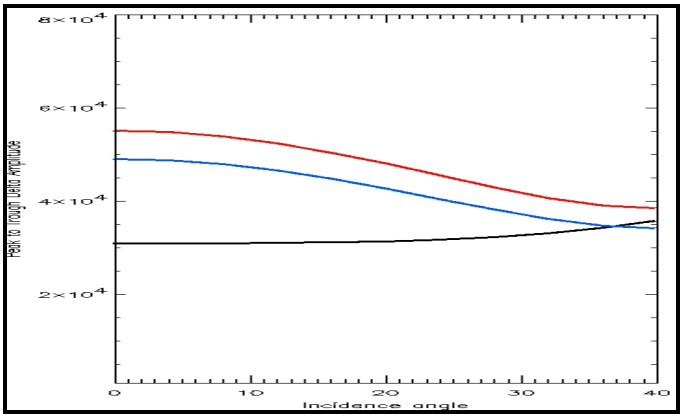

Figure 2: AVO response for the base case (in black) and the monitor case before (in blue) and after (in red) stretch

A significant advantage of this 4D inversion approach is that the amplitude and phase spectra for the base and monitor seismic data are not artificially modified to compensate for time-variant shifts and 4-D tuning effects are preserved.

The cumulated time shift maps between the base and the monitor obtained by classical cross correlation techniques and using the 4D inversion method are shown in Figure 3 and illustrate the benefit of this new technique which provides more details for interpretation

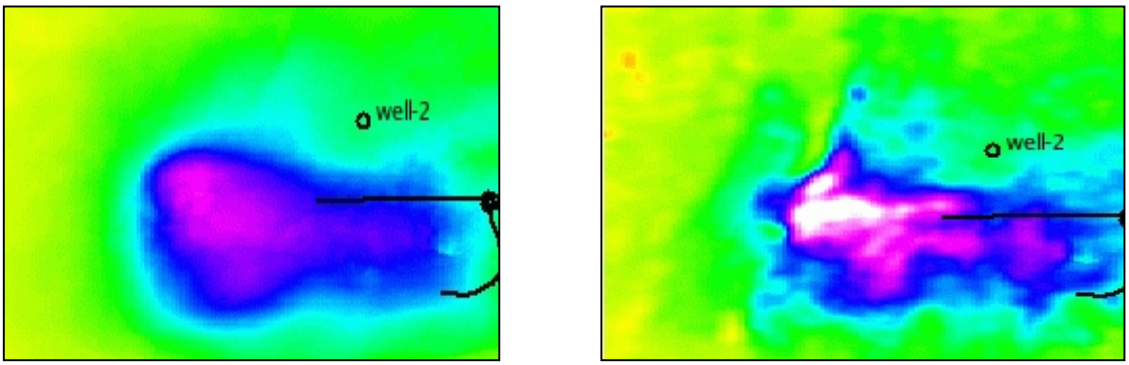

Figure 3: Time shift between the base and monitor obtained using a standard cross correlation technique (left) and after a 4D inversion (right)

PP/PS example

The new joint inversion without prior registration was tested on a 2D seismic dataset of a shale gas play from Canada. Five PP and PS angle stacks are available with P-incidence angles up to 35°. Figures 4a and 4b show one of the angle stacks for PP and PS data respectively. The PS data are not registered and are depicted in native PS time domain. The red horizons correspond to the first and last layers of the stratigraphic grid in PP and PS times. They define the inversion time window. Figures 4c and 4d respectively show the inverted I_P and V_P/V_S at the vertical well located along the section. The shale reservoir interval is associated with a strong increase in V_P/V_S. Three sets of inversion results are compared in the figure: PP only inversion (green), joint PP-PS inversion with prior registration (blue) and without prior registration (red). All results are comparable in terms of I_P (or slightly worse for the PP only inversion) but show more variability in the V_P/V_S estimates. The V_P/V_S ratio from the PP inversion is consistent with the well log at the target but the contrasts above and below are

underestimated, making the target more difficult to detect. The V_P/V_S ratio from the standard joint inversion is overestimated. In comparison, the new joint inversion without prior data registration provides a better fit at the target.

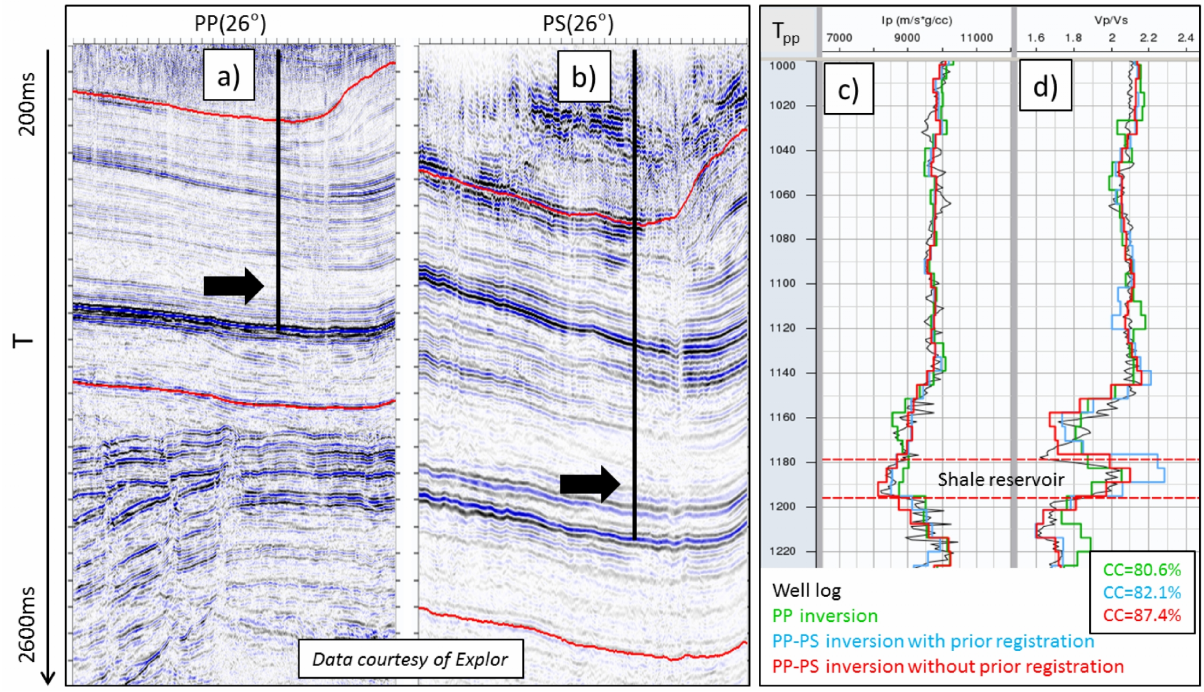

Figure 4: (a) PP and (b) PS angle stacks displayed in PP and PS time, respectively, with red horizons corresponding to the inversion window. Arrows indicate position of shale target along vertical well. (c) I_P and (d) V_P/V_S results from different inversions are displayed together with the corresponding well logs. The correlation coefficients, CC, between the inverted V_P/V_S ratios and the well log are also displayed.

Figure 5 illustrates how the new inversion simultaneously satisfies the amplitude and travel time information in addition to matching the well data as seen on Figure 4. Figures 5a and 5b show respectively corresponding PP and PS seismic traces extracted from the angle stacks displayed in Figure 4. Coloured markers identify the same events extracted from the stratigraphic grid in PP and PS times to illustrate the difference in travel times. Figures 5c and 5d depict the same traces after zooming, together with the corresponding synthetic traces from the PP inversion (green) and the new joint inversion (red). Both inversions show a good match to the PP seismic data in PP time (Figure 5c) but quite a different match to the PS seismic data in PS times (Figure 5d). The quality of the PP inversion can be judged by how well it predicts the PS data. The conversion to PS time in that case was done using the V_P/V_S ratio from the PP inversion. The combination of V_P, V_S and ρ estimated from the PP inversion poorly matches the PS seismic data in terms of amplitudes but also in terms of travel times. The time-shift between real and synthetic PS data reaches about 5 ms around 1575 ms and 2075 ms. In contrast, the new joint inversion provides estimates of V_P, V_S and ρ that match both amplitude and travel time simultaneously, i.e. only low PS residual amplitudes and time-shifts are observable.

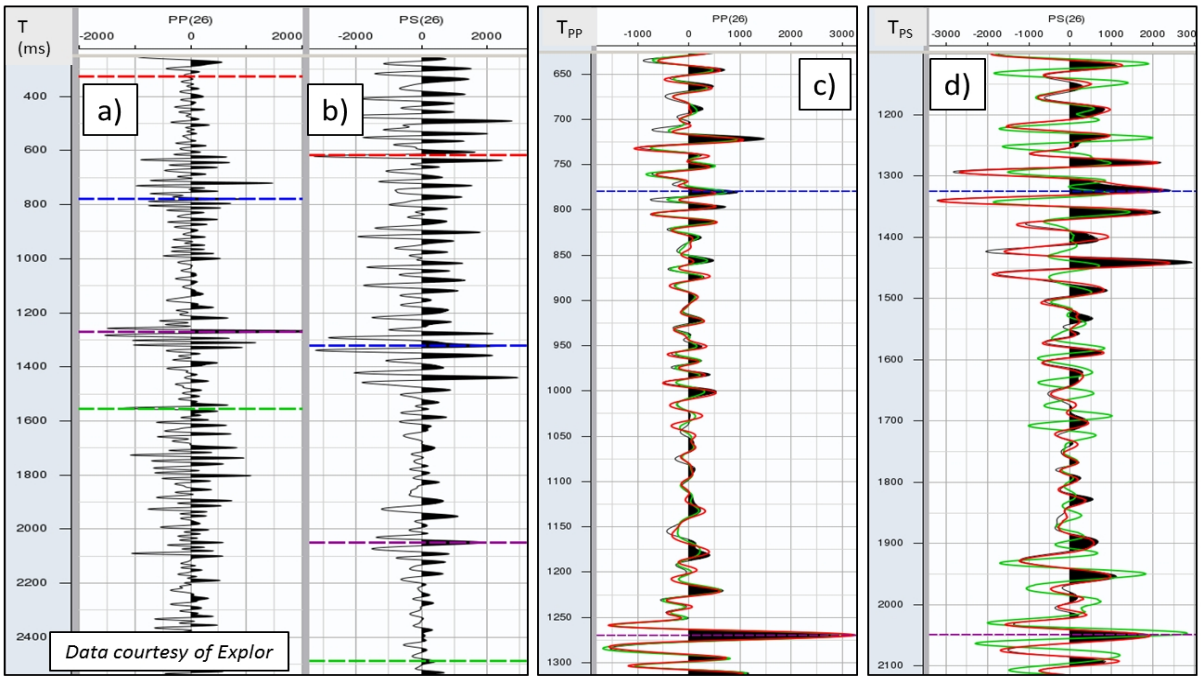

Figure 5: Real dataset inversion results. (a) PP seismic trace and (b) PS seismic trace with different time scales visualized by coloured markers, (c) zoom on the PP seismic trace (black) in PP time together with the synthetic traces from the PP inversion (green) and joint inversion (red), (d) zoom on the PS seismic trace (black) in PS time together with the synthetic traces from the PP inversion (green) and joint inversion (red).

Conclusions

The innovative inversion scheme is able to handle several seismic data with different time axis. This allows limiting the negative impact of time registration errors and registration-induced PS amplitude distortion. In 4D inversion the amplitude and phase spectra for the base and monitor seismic data are not artificially modified to compensate for time-variant shifts and 4-D tuning effects are preserved. The benefits of the new method were illustrated on a shale gas dataset from Canada and on a 4D example.

Acknowledgements

The authors would like to thank Philippe Doyen and Dave Tam for their contribution and Explor for permission to show the real data example.

References

Anderson, P.F. and Lines, L.R. [2008] A comparison of inversion techniques for estimating V_P/V_S from 3D seismic data. *CREWES Research Report*, **20**.

Aki, K. and Richards, P.G. [1980] *Quantitative Seismology, 2nd edition*. University Science Books.

Coulon, J.-P., Lafet, Y., Deschizeaux, B., Doyen, P. M. and Duboz, P. [2006] Stratigraphic elastic inversion for seismic lithology discrimination in a turbiditic reservoir. *SEG Expanded Abstracts*, 2092-2096.

Gray, F.D. [2003] P-S Converted-Wave AVO. *SEG Expanded Abstracts*, 165-168.

Lafet, Y., Roure, B., Doyen, P.D. and Buran, H. [2009] Global 4-D seismic inversion and time-lapse fluid classification. *SEG Expanded Abstracts*, 3830-3834.

Michou, L., Coleou, T., Lafet, Y. and Roure, B. [2013] 4D Seismic Inversion on Continuous Land Seismic Reservoir Monitoring of Thermal EOR. *GeoConvention*, Extended Abstracts.

Roure, B., Souvannavong, V., Coulon, J.-P. and Hampson, D. [2015] Joint PP-PS inversion without prior data registration, *77th EAGE Conference and Exhibition*, Extended Abstract, Tu N116 04.

Zoeppritz, K. [1919] Erdbebenwellen VIII B, Über die Reflexion und Durchgang seismischer Wellen durch Unstetigkeitsflächen. *Gottinger Nachr. 1*, 66-84.